Sphinx Journal of Mathematical Sciences
1(2), 72–93, 2026
DOI: https://doi.org/10.64389/sjms.2026.012120
https://sphinxsp.org/journal/index.php/sjms/

Research article

Stochastic Effect on Wave Propagation in Micro-elongated Thermoelastic Media under the Refined Dual-Phase-Lag Model With Multiplicative White Noise

Muhammad Abuzar[1,*], **Hazem Elsadek**[2],

[1] School of Mathematical Sciences, Guizhou Normal University, Guiyang, Yunyan 550003, China

[2] Department of computer science, Faculty of Computers and Information Systems,Egyptian Chinese University, Cairo, Egypt

* **Correspondence:** muhammadabuzar505@gmail.com

ARTICLE INFO

Keywords:
Refined Dual-Phase-Lag Model;
Stochastic system;
Micro-elongated;
Wiener Process

Mathematics Subject Classification:
74A15, 74A18, 93E03.

Important Dates:
Received: 23 May 2026
Revised: 17 June 2026
Accepted: 20 June 2026
Online: 24 June 2026

ABSTRACT

This study conducts a comprehensive investigation of stochastic effects on wave propagation in a micro-elongated thermoelastic medium within the frameworks of the Lord–Shulman theory (LST), the Dual-Phase-Lag model (DPLM), and the Refined Dual-Phase-Lag model (RDPLM). Through the application of an appropriate nondimensionalization procedure combined with an effective transform technique, the initially complex system of coupled stochastic partial differential equations is systematically reduced to a set of stochastic ordinary differential equations, from which explicit analytical solutions are obtained. The derived solutions offer valuable insight into the dynamic response of the medium, including displacement components, micro-elongation evolution, stress fields, and temperature variations. Consequently, the proposed formulation provides a unified and self-consistent framework for describing thermo-mechanical wave propagation. In addition, extensive numerical simulations are carried out to compare deterministic results with their stochastic counterparts. These comparisons demonstrate that random thermal disturbances significantly influence key wave characteristics, such as amplitude, attenuation, and propagation behavior, underscoring the crucial role of stochasticity in realistic thermoelastic wave modeling.

1. Introduction

The RDPLM constitutes a notable progression in non-Fourier heat conduction theories, introduced to remedy the intrinsic shortcomings of the conventional DPLM. While the DPLM incorporates finite thermal propagation through two relaxation times corresponding to the phase lags of the heat flux and the temperature gradient, it has been demonstrated to be inadequate for accurately modeling ultra-fast thermal processes prevalent in contemporary micro-scale applications. To address these limitations, the RDPLM augments the classical DPLM by incorporating higher-order correction terms and by providing a more rigorous formulation of the phase-lag parameters within the constitutive heat conduction relation [25, 16]. These enhancements improve the physical fidelity of the model by yielding a more realistic description of finite-speed heat transfer mechanisms. As a result, the RDPLM successfully captures wave-like thermal transport behavior, wherein heat propagation occurs with finite delays rather than instantaneous diffusion [1, 17]. Moreover, this refined framework effectively overcomes several deficiencies associated with the standard DPLM, such as non-physical instabilities and unrealistic temperature overshoots or peak values that frequently arise under ultra-fast thermal excitation [13, 26]. By suppressing these anomalies, the RDPLM ensures stable and physically consistent thermal responses. Comprehensive discussions of the theoretical formulation and practical relevance of the RDPLM are available in [6, 10]. Owing to these merits, the RDPLM has attracted growing interest in the analysis of thermoelastic phenomena, particularly in micro-scale systems.

Stochastic thermoelasticity represents an advanced generalization of classical and generalized thermoelastic theories, wherein both mechanical and thermal responses are explicitly modeled to account for randomness. In practical engineering applications and natural physical systems, uncertainty is unavoidable and may originate from numerous sources, such as spatial variations in material properties, microstructural defects, manufacturing tolerances, environmental disturbances, random thermal excitations, measurement errors, and time-varying or fluctuating mechanical loads. Traditional deterministic thermoelastic models generally overlook these intrinsic uncertainties, often yielding idealized predictions that fail to capture the complex behavior of real materials. To overcome this limitation, stochastic thermoelastic formulations incorporate randomness directly into the governing heat conduction equation, typically through the introduction of stochastic parameters or noise-driven processes, including Wiener-type stochastic excitations [7, 8] and white-noise perturbations [12, 23]. Within this probabilistic framework, the theory extends beyond the prediction of mean system responses to characterize the variability, dispersion, and temporal evolution of thermo-mechanical fields under uncertain conditions. As a result, key physical quantities such as displacement, temperature, and stress are treated as random fields whose statistical properties depend on both deterministic system parameters and the intensity and nature of the stochastic disturbances. Extensive theoretical developments and applications of stochastic thermoelasticity have been documented in the literature [3, 24]. These stochastic approaches are particularly effective for analyzing complex materials and systems in which randomness plays a significant role, including composite materials, microstructured and functionally graded solids, porous and biological media, and structures exposed to fluctuating thermal environments [19, 20, 22]. By capturing effects such as noise-induced damping and altered wave dispersion characteristics, stochastic thermoelasticity offers valuable insights for accurate modeling, robust design, and reliability assessment of structures operating under uncertain and variable conditions.

Micro-elongated thermoelastic media represent a specialized class of generalized continuum theories formulated to extend classical elasticity by incorporating additional deformation mechanisms arising from the material's internal microstructure [2, 18]. Unlike conventional thermoelastic models, which primarily describe macroscopic displacement fields and temperature variations, the micro-elongated framework introduces an extra kinematic variable that captures microscopic stretching or extension within the material. This internal deformation can be associated with the elongation of embedded fibers, stretching of molecular chains, rearrangement of internal structural elements, or relative extension among micro-scale particles. By explicitly accounting for these micro-level degrees of freedom, micro-elongated thermoelasticity provides a more comprehensive and physically realistic description of complex materials in which internal constituents are capable of independent deformation and significantly influence the overall mechanical and thermal behavior [11, 9]. Typical examples include polymers, biological tissues, fiber-reinforced composites, porous materials, and a broad range of engineered microstructured solids. When thermal effects are incorporated, the micro-elongation field interacts strongly with the temperature distribution, giving rise to additional stress components, modified constitutive relations, and new mechanisms of energy exchange that are not present in classical thermoelastic theories. Owing to these couplings, the wave propagation characteristics, stress profiles, and temperature evolution in micro-elongated media exhibit distinctive features such as enhanced dispersion, increased attenuation, and pronounced relaxation effects, all of which are governed by the underlying microstructural properties. Detailed theoretical treatments and applications of these phenomena have been extensively reported in the literature [4, 14, 15]. Consequently, micro-elongated thermoelastic theory plays a vital role in analyzing thermo-mechanical interactions and wave dynamics in advanced materials where classical formulations are inadequate.

This work investigates the combined effects of stochastic disturbances on the thermoelastic behavior of a micro-elongated half-space within the theoretical frameworks of the LST, DPLM, and its refined extension, the RDPLM. The analysis begins with the formulation of the fundamental governing equations that describe the coupled interactions among mechanical deformation, heat conduction, and micro-elongation in the medium. For analytical convenience and clarity, these equations are expressed in a dimensionless form. By applying the transform defined in Eq. (3.1), the resulting system of coupled stochastic partial differential equations is systematically reduced to a manageable set of stochastic ordinary differential equations. The unknown constants are then determined by enforcing the prescribed boundary conditions at $z = 0$, thereby completing the analytical solution process. The obtained solutions are subsequently employed to perform comprehensive numerical simulations and graphical analyses. These results provide detailed insight into the influence of stochastic excitations on the spatial distributions of key physical quantities, including displacement, temperature, stress components, and micro-elongation, within the micro-elongated thermoelastic medium.

2. Governing Equations

This section presents the fundamental governing equations of two-dimensional micro-elongated stochastic thermoelasticity under the LST, DPLM, and RDPLM frameworks. For analytical convenience, these equations are then expressed in a nondimensional form

The equation of motion can be given as follows:

$$\sigma_{ij,i} = \rho u_{i,tt}, \tag{2.1}$$

where

$$\sigma_{ij} = (\lambda e - \beta_0 \Theta + \lambda_0 \psi)\, \delta_{ij} + 2\mu\varepsilon_{ij}. \tag{2.2}$$

The equation of micro-elongated can be expressed as follows

$$a_0\psi_{,ii} - \lambda_1\psi + \beta_1\Theta - \lambda_0 u_{j,j} = \frac{\rho j^*\psi_{,tt}}{2}. \tag{2.3}$$

The energy equation can be expressed as follows [17, 7]:

$$\begin{aligned} 0 &= k\left(1 + \Sigma_{m=1}^{M}\frac{\tau_\theta^m}{(m)!}\frac{\partial^m}{\partial t^m}\right)\Theta_{,ii} - \beta_1 T_0\psi_{,t} + \frac{\nu\Theta_{,x}}{T_0}\frac{dW(t)}{dt} \\ &\quad -\left(1 + \Sigma_{m=1}^{M}\frac{\tau_q^m}{(m)!}\frac{\partial^m}{\partial t^m}\right)\left[\beta_0 T_0\left(u_{,xt} + w_{,zt}\right) + \rho c_e\Theta_{,t}\right], \end{aligned} \tag{2.4}$$

When
1- $M = 3$ and ($\tau_\theta < \tau_q \neq 0$, $k \neq 0$) is RDPM,
2- $M = 1$ and ($\tau_\theta < \tau_q \neq 0$, $k \neq 0$) is DPLM,
3- $M = 1$ and ($\tau_\theta = 0$, $\tau_q \neq 0$, $k \neq 0$) is LST.
where, $W(t)$ represents the Wiener process, while $\frac{dW(t)}{dt}$ white noise, and ν denotes the intensity of the white noise acting on the system.
The Wiener process is distinguished by several essential statistical features, which are given below [21, 5]:
i: For $t > \iota$, $W(t) - W(\iota)$ has independent increments.
ii: For $t \geq 0$, $W(t)$ has continuous trajectories.
iii: $W(t) - W(\iota)$ has a normal distribution with variance $= t - \iota$ and mean $= 0$.
Utilizing Eq. (2.2) in Eq. (2.1) with the aid of the displacement vector $\mathbf{u}(x, z, t) = u(u, 0, w)$, we get

$$\mu\nabla^2 u + (\lambda + \mu)e_{,x} - \beta_0\Theta_{,x} + \lambda_0\psi_{,x} = \rho u_{,tt}, \tag{2.5}$$

$$\mu\nabla^2 w + (\lambda + \mu)e_{,z} - \beta_0\Theta_{,z} + \lambda_0\psi_{,z} = \rho w_{,tt}. \tag{2.6}$$

Using the displacement vector $\mathbf{u}(x, z, t) = u(u, 0, w)$ in Eq. (2.3), one acquires

$$a_0\psi_{,ii} + \beta_1\Theta - \lambda_1\psi - \lambda_0\left(u_{,x} + w_{,z}\right) = \frac{\rho j^*\psi_{,tt}}{2}. \tag{2.7}$$

In our analysis, we utilize the following set of non-dimensional variables to simplify the equations and facilitate a more comprehensive understanding of the system's behavior

$$\begin{aligned} (u,\ v) &= \frac{T_0\beta_0}{\rho c_1\omega^*}(\bar{u},\ \bar{v}),\ (x, z) = \frac{c_1}{\omega^*}(\bar{x},\ \bar{z}),\ \Theta = T_0\bar{\Theta},\ \left(t,\ \tau_\theta,\ \tau_q\right) = \frac{\left(\bar{t},\ \bar{\tau}_\theta,\ \bar{\tau}_q\right)}{\omega^*},\ \sigma_{ij} = \beta_1 T_0\bar{\sigma}_{ij}, \\ \psi &= \frac{\beta_0 T_0}{\lambda_0}\bar{\psi},\ k\omega^* = \rho c_1^2 c_e,\ \rho c_1^2 = \lambda + \mu. \end{aligned} \tag{2.8}$$

Using Eq. (2.8) in Eq. (2.5), one infers

$$\left(\zeta_1\nabla^2 - \frac{\partial^2}{\partial t^2} + \zeta_2\frac{\partial^2}{\partial x^2}\right)u + \zeta_2\frac{\partial^2 w}{\partial x\partial z} - \frac{\partial\Theta}{\partial x} + \frac{\partial\psi}{\partial x} = 0, \tag{2.9}$$

Implementing Eq. (2.8) in Eq. (2.6), we uncover

$$\zeta_2\frac{\partial^2 u}{\partial x\partial z} + \left(\zeta_1\nabla^2 - \frac{\partial^2}{\partial t^2} + \zeta_2\frac{\partial^2}{\partial z^2}\right)w - \frac{\partial\Theta}{\partial z} + \frac{\partial\psi}{\partial z} = 0, \tag{2.10}$$

Applying Eq. (2.8) in Eq. (2.7), we discover

$$\zeta_5 \frac{\partial u}{\partial x} + \zeta_5 \frac{\partial w}{\partial z} - \zeta_3 \Theta - \left(\nabla^2 - \zeta_4 - \zeta_6 \frac{\partial^2}{\partial t^2} \right) \psi = 0, \tag{2.11}$$

Inserting Eq. (2.8) in Eq. (2.4), one realizes

$$\zeta_8 \left(1 + \tau_2\right) \frac{\partial^2 u}{\partial x \partial t} + \zeta_8 \left(1 + \tau_2\right) \frac{\partial^2 w}{\partial z \partial t} - \left(\nabla^2 + \tau_1 \nabla^2 - \zeta_7 \frac{\partial}{\partial t} - \tau_2 \zeta_7 \frac{\partial}{\partial t} \right) \Theta + \frac{\nu c_1}{k T_0 \omega^*} \frac{\partial \Theta}{\partial x} \frac{dW\left(t\right)}{dt} + \zeta_9 \frac{\partial \psi}{\partial t} = 0, \tag{2.12}$$

where, $\zeta_1 = \frac{\mu}{c_1^2 \rho}$, $\zeta_2 = \frac{\mu + \lambda}{c_1^2 \rho}$, $\zeta_3 = \frac{\lambda_0 \beta_1 c_1^2}{\beta_0 a_0 \omega^{*2}}$, $\zeta_4 = \frac{c_1^2 \lambda_1}{a_0 \omega^{*2}}$, $\zeta_5 = \frac{\lambda_0^2}{a_0 \rho \omega^{*2}}$, $\zeta_6 = \frac{\rho j^* c_1^2}{2 a_0}$, $\zeta_7 = \frac{\rho c_e c_1^2}{k \omega^*}$, $\zeta_8 = \frac{\beta_0^2 T_0}{k \omega^* \rho}$, $\zeta_9 = \frac{\beta_0 \beta_1 T_0 c_1^2}{k \omega^* \lambda_0}$, $\tau_1 = \Sigma_{m=1}^{M} \frac{\tau_\theta^m}{m!} \frac{\partial^m}{\partial t^m}$, and $\tau_2 = \Sigma_{m=1}^{M} \frac{\tau_q^m}{m!} \frac{\partial^m}{\partial t^m}$.
Using Eq. (2.8) in Eq. (2.2), we find

$$\sigma_{xx} = \frac{\partial u}{\partial x} + \zeta_{10} \frac{\partial w}{\partial z} - \Theta + \psi, \tag{2.13}$$

$$\sigma_{zz} = \zeta_{10} \frac{\partial u}{\partial x} + \frac{\partial w}{\partial z} - \Theta + \psi, \tag{2.14}$$

$$\sigma_{zx} = \sigma_{xz} = \zeta_1 \frac{\partial u}{\partial z} + \zeta_1 \frac{\partial w}{\partial x}. \tag{2.15}$$

where, $\zeta_{10} = \frac{\lambda_0^2}{a_0 \rho \omega^{*2}}$.
The displacement potentials $\varpi\left(x, z, t\right)$ and $\eta\left(x, z, t\right)$ which relate to displacement components have been introduced,one receives

$$u = \varpi_{,x} + \eta_{,z}, \qquad w = \varpi_{,z} - \eta_{,x}. \tag{2.16}$$

Using Eq. (2.16) in Eqs. (2.9), (2.10), (2.11), and (2.12), we see

$$\left[\left(\zeta_1 + \zeta_2\right) \nabla^2 - \frac{\partial^2}{\partial t^2} \right] \varpi - \Theta + \psi = 0, \tag{2.17}$$

$$\left[\zeta_1 \nabla^2 - \frac{\partial^2}{\partial t^2} \right] \eta = 0, \tag{2.18}$$

$$\zeta_5 \nabla^2 \varpi - \zeta_3 \Theta - \left(\nabla^2 - \zeta_4 - \zeta_6 \frac{\partial^2}{\partial t^2} \right) \psi = 0, \tag{2.19}$$

$$\zeta_8 \left(1 + \tau_2\right) \nabla^2 \left(\frac{\partial \varpi}{\partial t} \right) - \left(\nabla^2 + \tau_1 \nabla^2 - \zeta_7 \frac{\partial}{\partial t} - \tau_2 \zeta_7 \frac{\partial}{\partial t} \right) \Theta + \frac{\nu c_1}{k T_0 \omega^*} \frac{\partial \Theta}{\partial x} \frac{dW\left(t\right)}{dt} + \zeta_9 \frac{\partial \psi}{\partial t} = 0. \tag{2.20}$$

3. Solution

The solution for the considered physical variables can be formulated and examined using a modal representation as follows:

$$\left[u,\ w,\ \Theta,\ \psi,\ \varpi,\ \eta,\ \sigma_{ij}\right]\left(x,\ z,\ t\right) = \left[\tilde{u},\ \tilde{w},\ \tilde{\Theta},\ \tilde{\psi},\ \tilde{\varpi},\ \tilde{\eta},\ \tilde{\sigma}_{ij}\right]\left(z\right) e^{i\left(\varsigma x - \omega t + \nu W(t) - \nu^2 t\right)}. \tag{3.1}$$

where, ς is the wave number and ω is the frequency.
Inserting Eq. (3.1) into Eqs. (2.17), (2.18), (2.19), and (2.20), we have

$$\left(\alpha_1 D^2 + \alpha_2\right)\tilde{\varpi} - \tilde{\Theta} + \tilde{\psi} = 0, \tag{3.2}$$

$$\left[\zeta_1 D^2 + \alpha_3\right]\tilde{\eta} = 0, \tag{3.3}$$

$$\left[\zeta_5 D^2 - \alpha_4\right]\tilde{\varpi} - \zeta_3\tilde{\Theta} - \left(D^2 + \alpha_5\right)\tilde{\psi} = 0, \tag{3.4}$$

$$\left[\alpha_6 D^2 - \alpha_7\right]\tilde{\varpi} - \left(\alpha_8 D^2 - \alpha_9\right)\tilde{\Theta} + \alpha_{10}\tilde{\psi} = 0, \tag{3.5}$$

where, $\alpha_1 = \zeta_1 + \zeta_2$, $\alpha_2 = \left(\omega + \nu^2 - \nu\frac{dW(t)}{dt}\right)^2 - \varsigma^2\alpha_1$, $\alpha_3 = \left(\omega + \nu^2 - \nu\frac{dW(t)}{dt}\right)^2 - \zeta_1\varsigma^2$,
$\alpha_4 = \varsigma^2\zeta_5$, $\alpha_5 = \zeta_6\left(\omega + \nu^2 - \nu\frac{dW(t)}{dt}\right)^2 - \zeta_4 - \varsigma^2$, $\alpha_6 = i\zeta_8\left(1 + \tau_2\right)\left(\nu\frac{dW(t)}{dt} - \omega - \nu^2\right)$, $\alpha_7 = \alpha_6\varsigma^2$,
$\alpha_8 = \left(1 + \tau_1\right)$, $\alpha_9 = \alpha_8\varsigma^2 + i\zeta_7\left(1 + \tau_2\right)\left(\omega + \nu^2 - \nu\frac{dW(t)}{dt}\right) - \frac{i\varsigma\nu c_1}{kT_0\omega^*}\frac{dW(t)}{dt}$, $\alpha_{10} = i\zeta_9\left(\nu\frac{dW(t)}{dt} - \omega - \nu^2\right)$.
It is observed that the cases

1. $\tau_1 = \left(\omega + \nu^2 - \nu\frac{dW(t)}{dt}\right)\tau_\theta\left[-i - \left(\omega + \nu^2 - \nu\frac{dW(t)}{dt}\right)\frac{\tau_\theta}{2} + i\left(\omega + \nu^2 - \nu\frac{dW(t)}{dt}\right)^2\frac{\tau_\theta^2}{6}\right]$ and
   $\tau_2 = \left(\omega + \nu^2 - \nu\frac{dW(t)}{dt}\right)\tau_q\left[-i - \left(\omega + \nu^2 - \nu\frac{dW(t)}{dt}\right)\frac{\tau_q}{2} + i\left(\omega + \nu^2 - \nu\frac{dW(t)}{dt}\right)^2\frac{\tau_q^2}{6}\right]$ correspond to the RDPLM
2. $\tau_1 = -i\left(\omega + \nu^2 - \nu\frac{dW(t)}{dt}\right)\tau_\theta$ and $\tau_2 = -i\left(\omega + \nu^2 - \nu\frac{dW(t)}{dt}\right)\tau_q$ correspond to the DPLM
3. $\tau_1 = 0$ and $\tau_2 = -i\left(\omega + \nu^2 - \nu\frac{dW(t)}{dt}\right)\tau_q$ correspond to the LST

Equations (3.2), (3.4), and (3.5) yield a nontrivial solution when the determinant of the coefficient matrix associated with the physical quantities equals zero. Using the MATLAB program, we infer

$$\left(D^6 - B_1 D^4 + B_2 D^2 - B_3\right)\{\tilde{\varpi}(z),\ \tilde{\Theta}(z),\ \tilde{\psi}(z)\} = 0, \tag{3.6}$$

where, $B_1 = \frac{1}{\alpha_1\alpha_8}\{\alpha_6 + \alpha_1\alpha_9 - \alpha_2\alpha_8 - \zeta_5\alpha_8 - \alpha_1\alpha_5\alpha_8\}$,
$B_2 = \frac{-1}{\alpha_1\alpha_8}\{-\alpha_7 + \alpha_2\alpha_9 + \alpha_5\alpha_6 + \alpha_4\alpha_8 + \alpha_6\zeta_3 + \alpha_9\zeta_5 + \alpha_{10}\zeta_5 + \alpha_1\alpha_5\alpha_9 - \alpha_2\alpha_5\alpha_8 - \alpha_1^2\}$,
$B_3 = \frac{1}{\alpha_1\alpha_8}\{-\alpha_7\zeta_3 - \alpha_5\alpha_7 - \alpha_4\alpha_9 - \alpha_4\alpha_{10} + \alpha_2\alpha_5\alpha_9 - \alpha_2\alpha_{10}\zeta_3\}$.
This equation can be written as

$$\left(D^2 - r_1\right)\left(D^2 - r_2\right)\left(D^2 - r_3\right)\{\tilde{\varpi}(z),\ \tilde{\Theta}(z),\ \tilde{\psi}(z)\} = 0, \tag{3.7}$$

where, r_1, r_2, and r_3 are roots
The general solution of Eq. (3.7) bound as $z \to \infty$ can be expressed as

$$\tilde{\varpi}(z) = \Sigma_{n=1}^{3} L_n e^{-r_n z}, \tag{3.8}$$
$$\tilde{\psi}(z) = \Sigma_{n=1}^{3} \Xi_{1n} L_n e^{-r_n z}, \tag{3.9}$$
$$\tilde{\Theta}(z) = \Sigma_{n=1}^{3} \Xi_{2n} L_n e^{-r_n z}, \tag{3.10}$$

where, $\Xi_{1n} = \frac{(\zeta_5 - \zeta_3\alpha_1)r_n^2 - (\zeta_3\alpha_2 + \alpha_4)}{r_n^2 + \zeta_3 + \alpha_5}$, $\Xi_{2n} = \alpha_1 r_n^2 + \alpha_2 + \Xi_{1n}$.
The general solution of Eq. (3.3) bound as $z \to \infty$ can be written as

$$\tilde{\eta}(z) = He^{-Sz}, \tag{3.11}$$

where $S = \sqrt{\frac{-\alpha_3}{\zeta_1}}$.
Employing Eq. (3.1) in Eq. (2.16), then using Eqs. (3.8) and (3.11), one obtains

$$\tilde{u} = i\varsigma\Sigma_{n=1}^{3} L_n e^{-r_n z} - S H e^{-S z}, \tag{3.12}$$
$$\tilde{w} = -\Sigma_{n=1}^{3} r_n L_n e^{-r_n z} - i\varsigma H e^{-S z}. \tag{3.13}$$

Using Eq. (3.1) into Eqs. (2.13), (2.14), and (2.15), then employing Eqs. (3.9), (3.10), (3.12) and (3.13), one infers

$$\tilde{\sigma}_{xx} = \Sigma_{n=1}^{3} \Xi_{3n} L_n e^{-r_n z} + i\varsigma (\zeta_{10} - 1) S H e^{-S z}, \tag{3.14}$$
$$\tilde{\sigma}_{zz} = \Sigma_{n=1}^{3} \Xi_{4n} L_n e^{-r_n z} + i\varsigma (1 - \zeta_{10}) S H e^{-S z}, \tag{3.15}$$
$$\tilde{\sigma}_{xz} = \tilde{\sigma}_{zx} = \Sigma_{n=1}^{3} \Xi_{5n} L_n e^{-r_n z} + \zeta_1 \left(S^2 + \varsigma^2\right) H e^{-S z}, \tag{3.16}$$

where, $\Xi_{3n} = \zeta_{10} r_n^2 - \varsigma^2 + \Xi_{1n} - \Xi_{2n}$, $\Xi_{4n} = r_n^2 - \zeta_{10}\varsigma^2 + \Xi_{1n} - \Xi_{2n}$, $\Xi_{5n} = -2i\varsigma\zeta_1 r_n$.

4. Boundary condition

To find the constants (L_1, L_2, L_3, and H), we have applied the boundary conditions for the problem at $z = 0$ as follows:

$$\sigma_{xz} = 0, \ \sigma_{zz} = f_1 e^{i\left(\varsigma x - \omega t + \nu W(t) - \nu^2 t\right)}, \ \frac{\partial \psi}{\partial z} = 0, \ \Theta = f_2 e^{i\left(\varsigma x - \omega t + \nu W(t) - \nu^2 t\right)}, \tag{4.1}$$

where f_1 represents the amplitude of force being applied and f_2 is a constant.
Substituting the assumed expressions of the field variables into the previously defined boundary conditions (4.1) yields a set of algebraic relations that must be satisfied by the associated parameters. Consequently, a system of four equations is obtained. This system is solved using the inverse matrix approach to evaluate the unknown constants (L_1, L_2, L_3, and H) leading to explicit expressions for these quantities as given below.

$$\begin{bmatrix} L_1 \\ L_2 \\ L_3 \\ H \end{bmatrix} = \begin{bmatrix} \Xi_{51} & \Xi_{52} & \Xi_{53} & \zeta_1 S^2 + \zeta_1 \varsigma^2 \\ \Xi_{41} & \Xi_{42} & \Xi_{43} & i\varsigma (1 - \zeta_{10}) S \\ -r_1 \Xi_{11} & -r_2 \Xi_{12} & -r_3 \Xi_{13} & 0 \\ \Xi_{21} & \Xi_{22} & \Xi_{23} & 0 \end{bmatrix}^{-1} \begin{bmatrix} 0 \\ f_1 \\ 0 \\ f_2 \end{bmatrix} \tag{4.2}$$

5. Numerical discussions and results

This section provides a set of graphical illustrations of the obtained solutions in a two-dimensional context. These visualizations are essential for capturing the evolution of the key field variables, thereby improving the physical interpretation of the results and highlighting the qualitative behavior of the system. For the numerical analysis, an aluminum–epoxy composite is selected as the representative thermoelastic material due to its well-characterized thermal and mechanical properties, making it particularly suitable for studying coupled thermoelastic responses. The numerical values employed in the computations are summarized in the following [2]

$$\begin{aligned}
j^* &= 0.196\times 10^{-4}\ \mathrm{m}^2, \qquad \lambda = 7.59\times 10^{10}\,\frac{\mathrm{N}}{\mathrm{m}^2}, \qquad \rho = 2190\,\frac{\mathrm{kg}}{\mathrm{m}^3},\\
\mu &= 1.89\times 10^{10}\,\frac{\mathrm{N}}{\mathrm{m}^2}, \quad \beta_0 = 0.50\times 10^{5}\,\frac{\mathrm{N}}{\mathrm{m}^2.\mathrm{K}}, \quad \lambda_0 = 0.37\times 10^{10}\,\frac{\mathrm{N}}{\mathrm{m}^2},\\
\beta_1 &= 0.50\times 10^{5}\,\frac{\mathrm{N}}{\mathrm{m}^2.\mathrm{K}}, \qquad c_e = 966\,\frac{\mathrm{J}}{\mathrm{kg.K}}, \quad k = 252\,\frac{\mathrm{J}}{\mathrm{m.s.K}}, \quad T_0 = 293^\circ\ \mathrm{K},\\
\lambda_1 &= 0.37\times 10^{10}\,\frac{\mathrm{N}}{\mathrm{m}^2}, \qquad a_0 = 0.61\times 10^{-10}, \qquad \tau_\theta = 0.31\ \mathrm{s}, \quad \tau_q = 0.7\ \mathrm{s}\\
f_1 &= 1.201, \quad f_2 = 0.502.
\end{aligned}$$

In this work, the numerical simulations are performed for all physical quantities at the time $t = 0.6$ over along the surface $x = 0.5$. The employed numerical approach is utilized to describe and examine the behavior of the displacement components u, and w, the stress components σ_{zz}, σ_{xx}, and σ_{xz}, as well as the temperature field Θ, and the micro-elongation variable ψ. The resulting graphical results demonstrate the theoretical predictions of the LST, DPLM, and RDPLM. Figures 1, 2, 3, 4, 5, 6, and 7 provide a comprehensive comparison between deterministic and stochastic field responses within the RDPLM, emphasizing the effects of random thermal fluctuations on wave propagation in a micro-elongated thermoelastic medium. Figure 1 shows the horizontal displacement (u) distributions for the RDPLM. The deterministic response ($\nu = 0$) is a smooth curve, while the stochastic curves ($\nu = 2, 2.2, 2.4$) exhibit intense, high-frequency oscillations that decay as the depth (z) increases. Physically, this demonstrates that multiplicative white noise significantly disrupts the stability of mechanical wave propagation. Figure 2 clarifies the vertical displacement (w) distributions for the RDPLM. Similar to horizontal displacement, the noise-induced fluctuations are most violent near the boundary ($z = 0$) and gradually attenuate, showing how stochastic thermal effects modify the amplitude of mechanical responses. Figure 3 demonstrates the stress tensor (σ_{zz}) distributions for the RDPLM. The large random fluctuations for $\nu > 0$ indicate that thermal stochastic directly impacts the internal stress fields within the medium. Figure 4 illustrates the stress tensor (σ_{xx}) distributions for the RDPLM. This highlights the coupling between thermal noise and lateral mechanical tension, where the stochastic intensity (ν) dictates the magnitude of the stress variability. Figure 5 depicts the stress tensor (σ_{xz}) distributions for the RDPLM. The fluctuations represent noise-induced changes in the stress tensor (σ_{xz}) wave patterns, which are absent in the smooth deterministic model. Figure 6 displays the temperature (Θ) distributions for the RDPLM. In this model, stochastic thermal fluctuations manifest as random thermal waves rather than as simple instantaneous diffusion, reflecting the RDPLM's ability to describe heat propagation as a finite-speed wave. Figure 7 exhibits the micro-elongation (ψ) distributions for the RDPLM. The high sensitivity of ψ to the noise parameter ν confirms that the micro-elongated of material is deeply affected by stochastic thermal. Figures 8, 9, 10, 11, 12, 13, and 14 illustrate a systematic comparison of deterministic and stochastic responses under the DPLM, demonstrating how random thermal fluctuations alter wave propagation characteristics in a micro-elongated thermoelastic medium. Figure 8 reveals the horizontal displacement (u) distributions for the DPLM. While still oscillatory under noise, the response is generally less erratic than the RDPLM. Figure 9 appears the vertical displacement (w) distributions for the DPLM. The curves illustrate how stochastic thermal fluctuations influence wave propagation, with the noise attenuation exhibiting a more linear behavior compared to that observed in the RDPLM. Figure 10 depicts the stress tensor (σ_{zz}) distributions for the DPLM. The fluctuations around the deterministic baseline illustrate the dispersion of mechanical stress caused by stochastic effects. Figure 11 shows the stress tensor

(σ_{xx}) distributions for the DPLM. The curves demonstrate the variation in wave amplitude and attenuation as the intensity of the white noise increases. Figure 12 clarifies the stress tensor (σ_{xz}) distributions for the DPLM. The observed oscillations indicate the absence of a stable stress value under stochastic thermal excitations. Figure 13 demonstrates the temperature (Θ) distributions for the DPLM. The results exhibit a more conventional decay compared to the RDPLM, while still reflecting the variability introduced by the Wiener process. Figure 14 illustrates the micro-elongation (ψ) distributions for the DPLM. The interaction between thermal noise and the micro-elongated is visible, but the oscillations are slightly dampened compared to the refined model. Figures 15, 16, 17, 18, 19, 20, and 21 depict a detailed contrast between deterministic and stochastic field behaviors within the LST, revealing the role of random thermal disturbances in shaping wave propagation in a micro-elongated thermoelastic medium. Figure 15 displays the horizontal displacement (u) distributions for the LST. The deterministic response is relatively simple, and although stochastic is evident, it exhibits less wave-like dispersion compared to the phase-lag models. Figure 16 shows the vertical displacement (w) distributions for the LST. Physically, this reflects the theory's inherently diffusive character, which tends to moderate the more pronounced mechanical responses to thermal noise. Figure 17 depicts the stress tensor (σ_{zz}) distributions for the LST. The stress field exhibits a conventional pattern, with noise-induced fluctuations rather than the organized oscillatory behavior observed in the RDPLM. Figure 18 shows the stress tensor (σ_{xx}) distributions for the LST. The results confirm that the LST offers a more damped perspective on the effects of white noise in thermoelastic media. Figure 19 exhibits the stress tensor (σ_{xz}) distributions for the LST. The variability induced by noise is primarily localized near the boundary and stabilizes quickly. Figure 20 illustrates the temperature (Θ) distributions for the LST. It displays the weakest response to stochastic fluctuations among the three models. Figure 21 shows the micro-elongation (ψ) distributions for the LST. This reflects the minimal coupling between the micro-level degrees of freedom and the stochastic thermal field in this simpler framework.

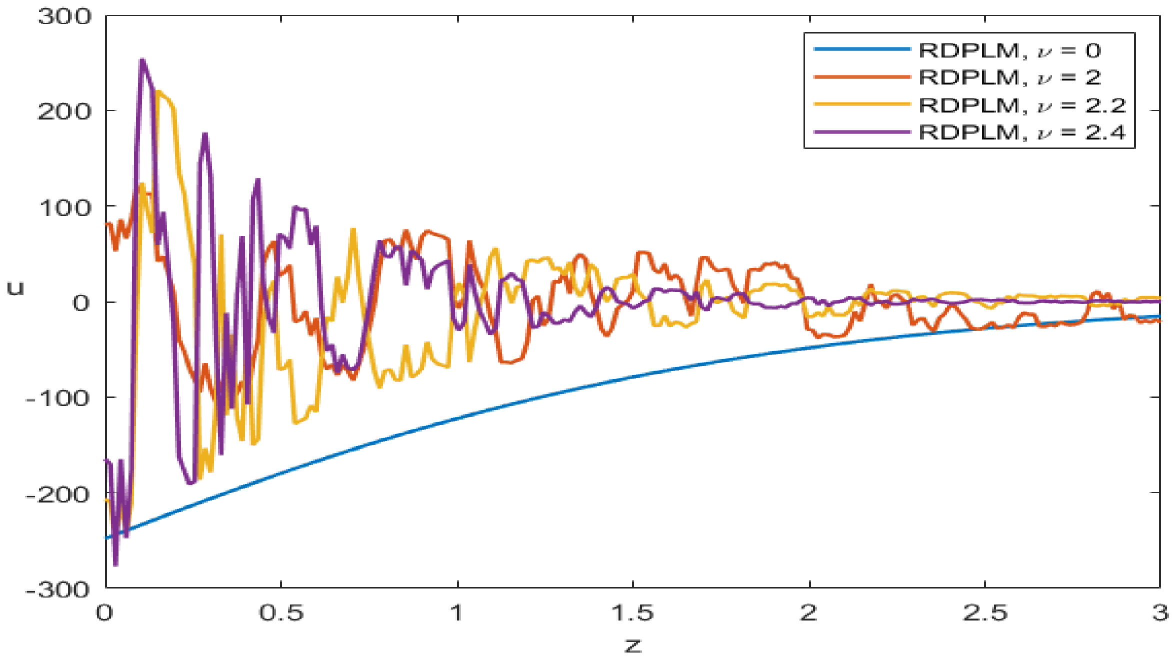

Figure 1. The horizontal displacement distributions for the RDPLM

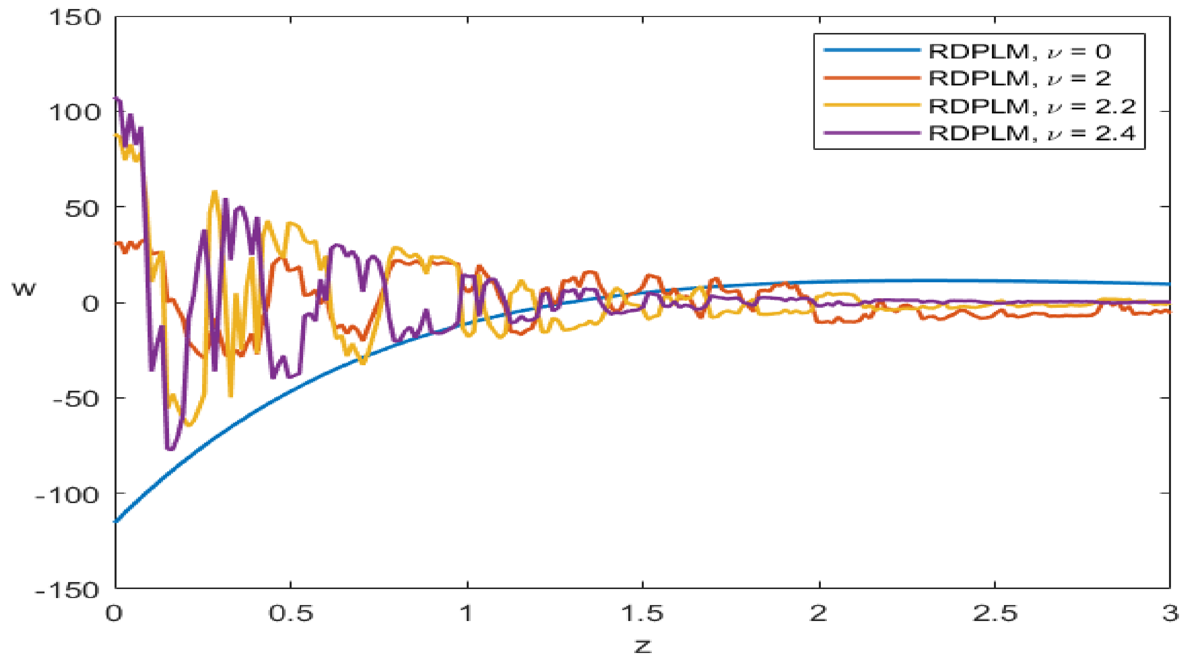

Figure 2. The vertical displacement distributions for the RDPLM

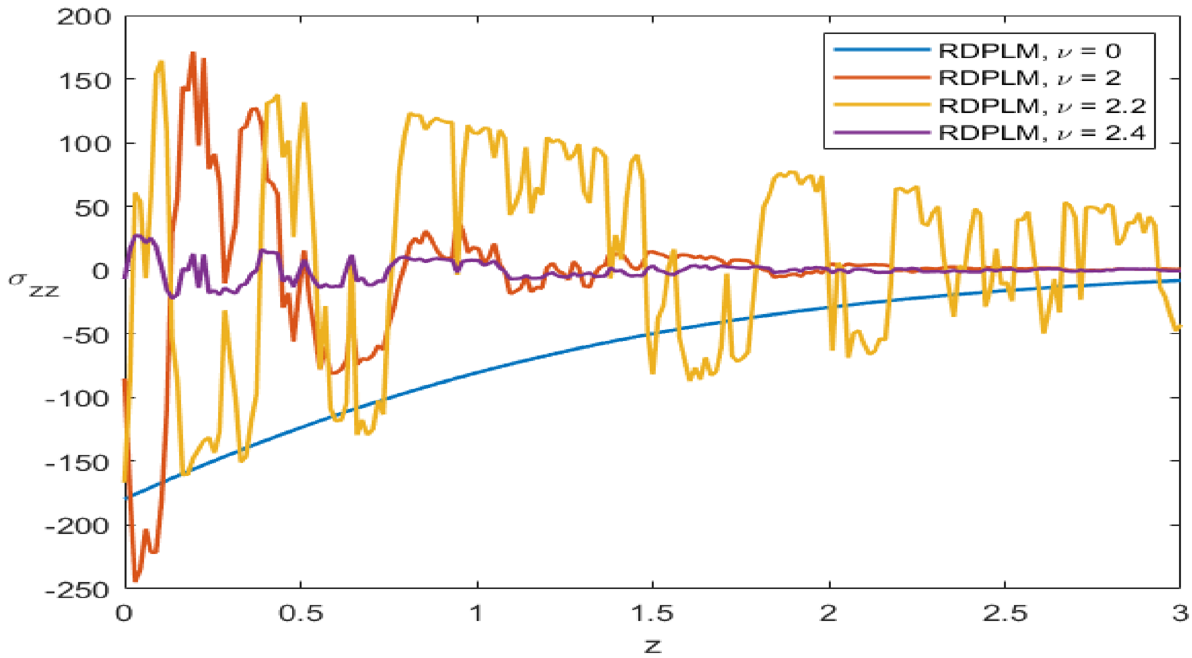

Figure 3. The stress tensor (σ_{zz}.) distributions for the RDPLM

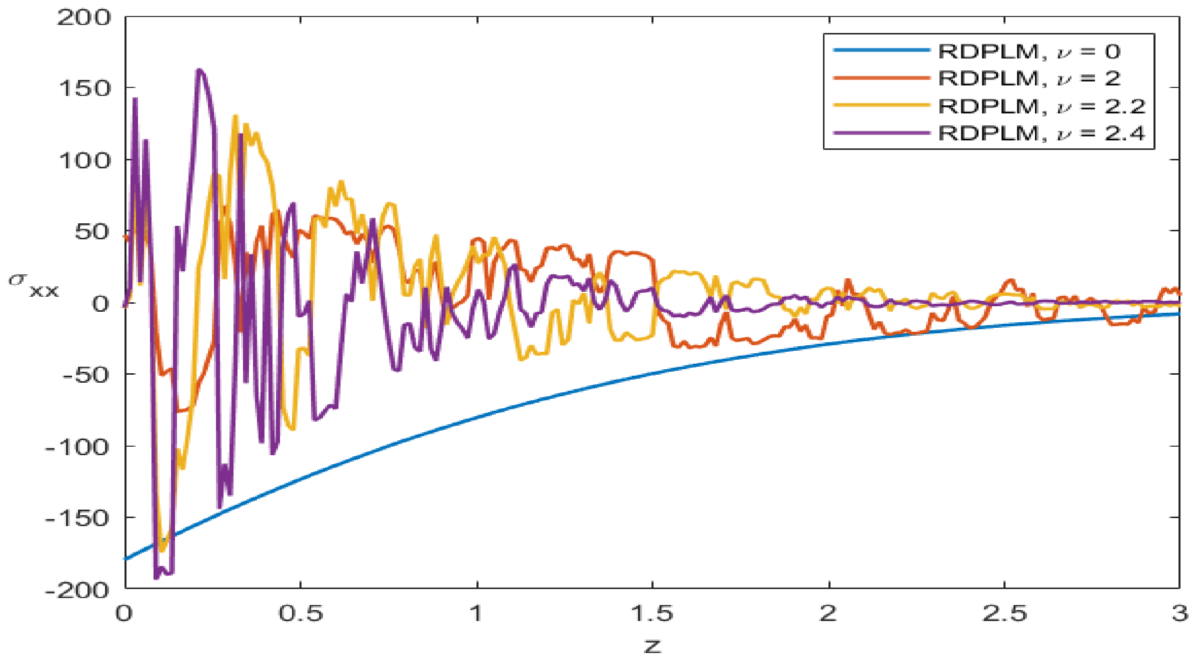

Figure 4. The stress tensor (σ_{xx}.) distributions for the RDPLM

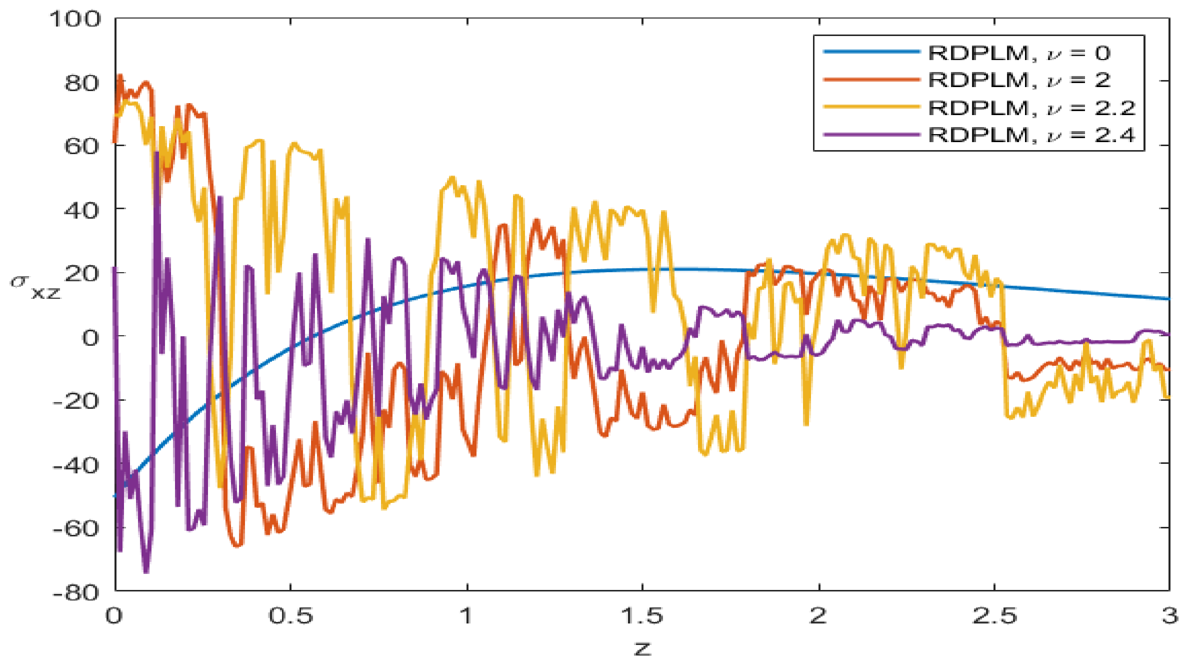

Figure 5. The stress tensor (σ_{xz}.) distributions for the RDPLM

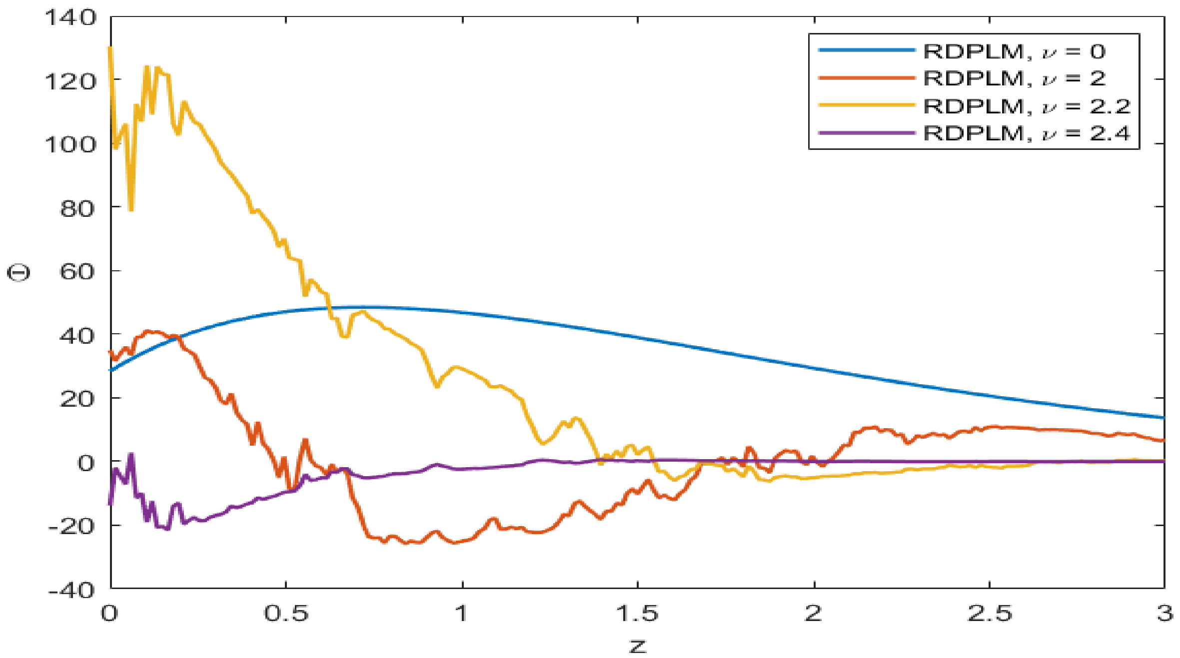

Figure 6. The temperature distributions for the RDPLM

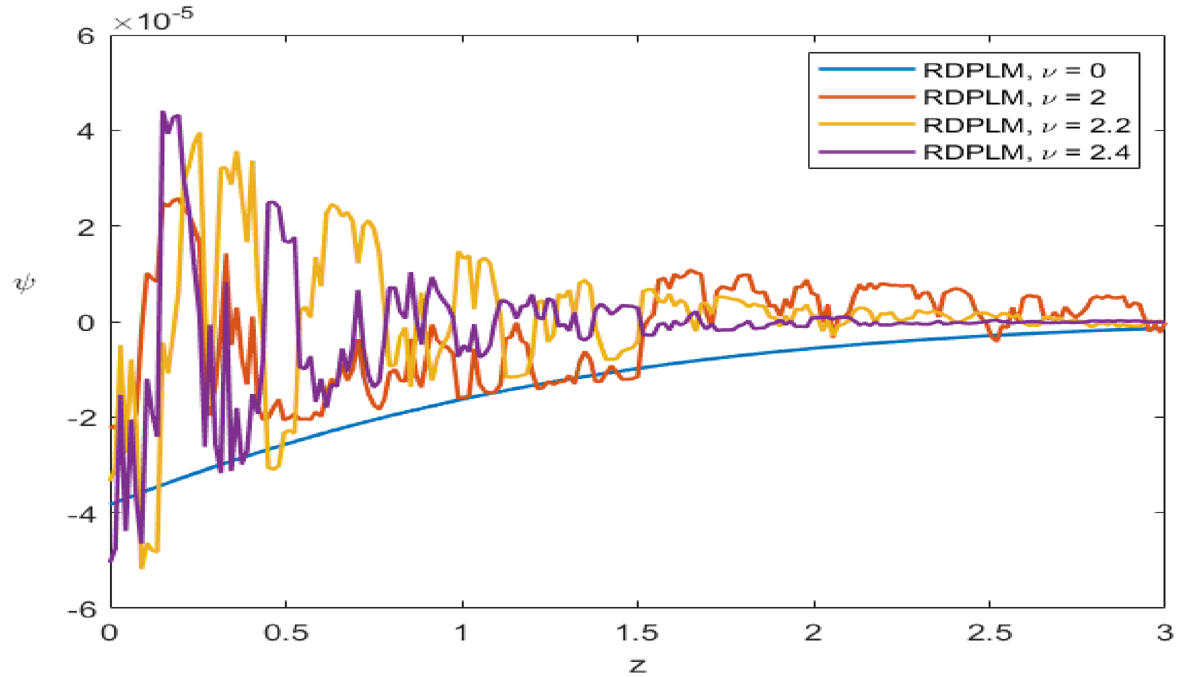

Figure 7. The micro-elongated distributions for the RDPLM

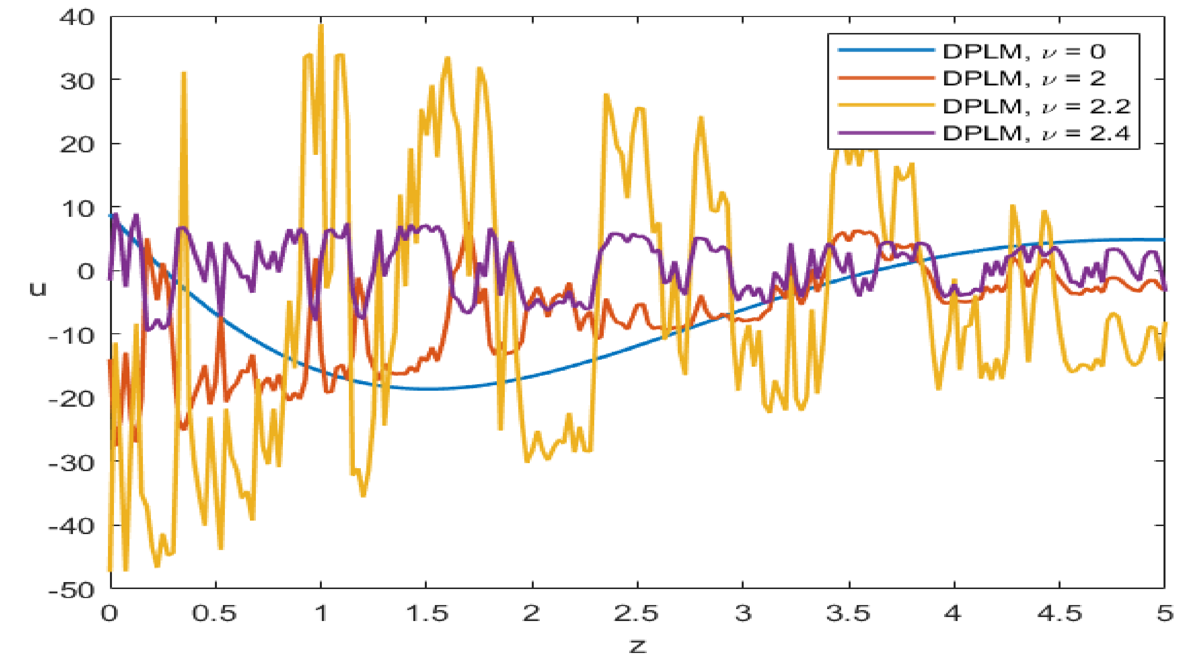

Figure 8. The horizontal displacement distributions for the DPLM

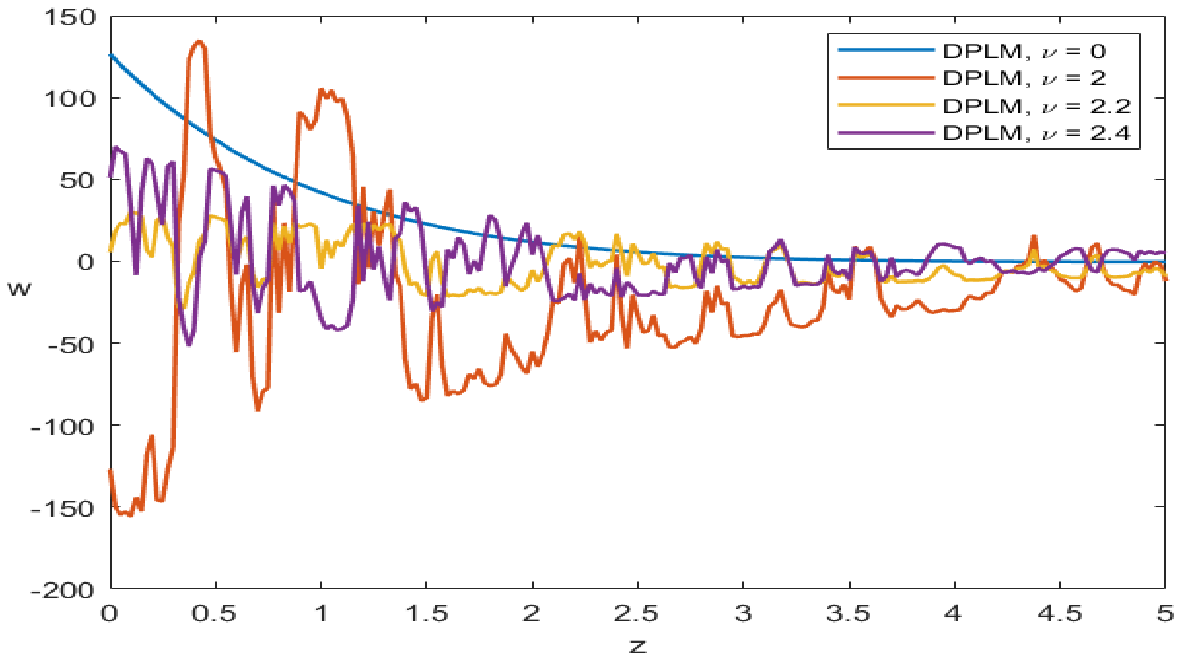

Figure 9. The vertical displacement distributions for the DPLM

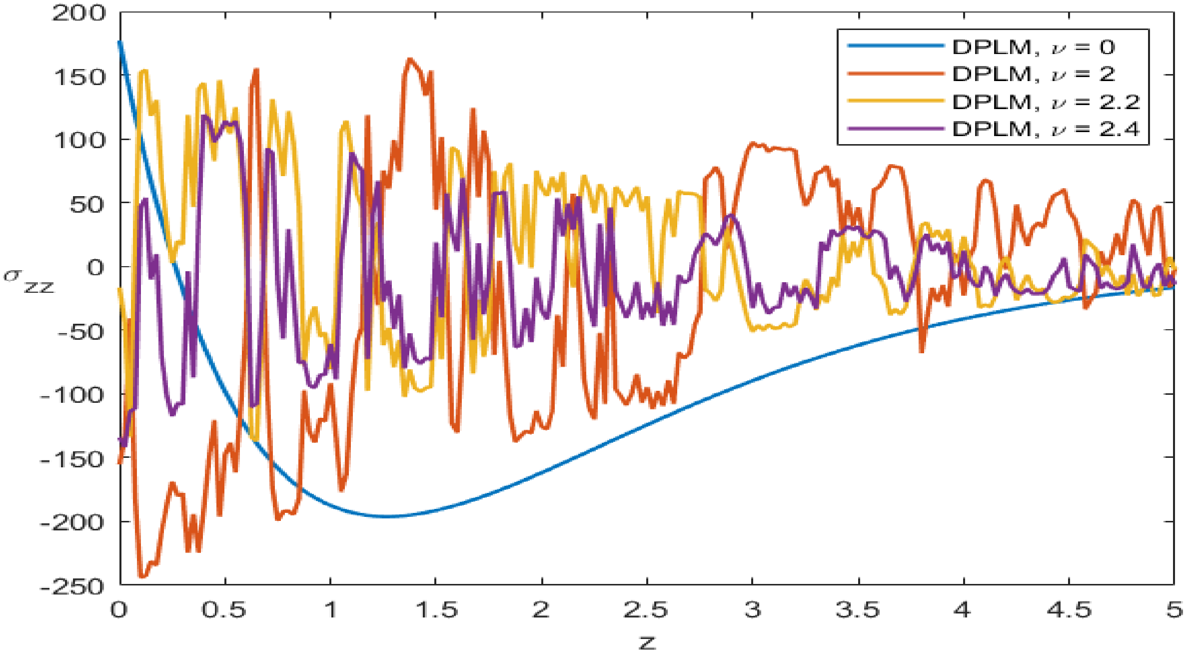

Figure 10. The stress tensor (σ_{zz}.) distributions for the DPLM

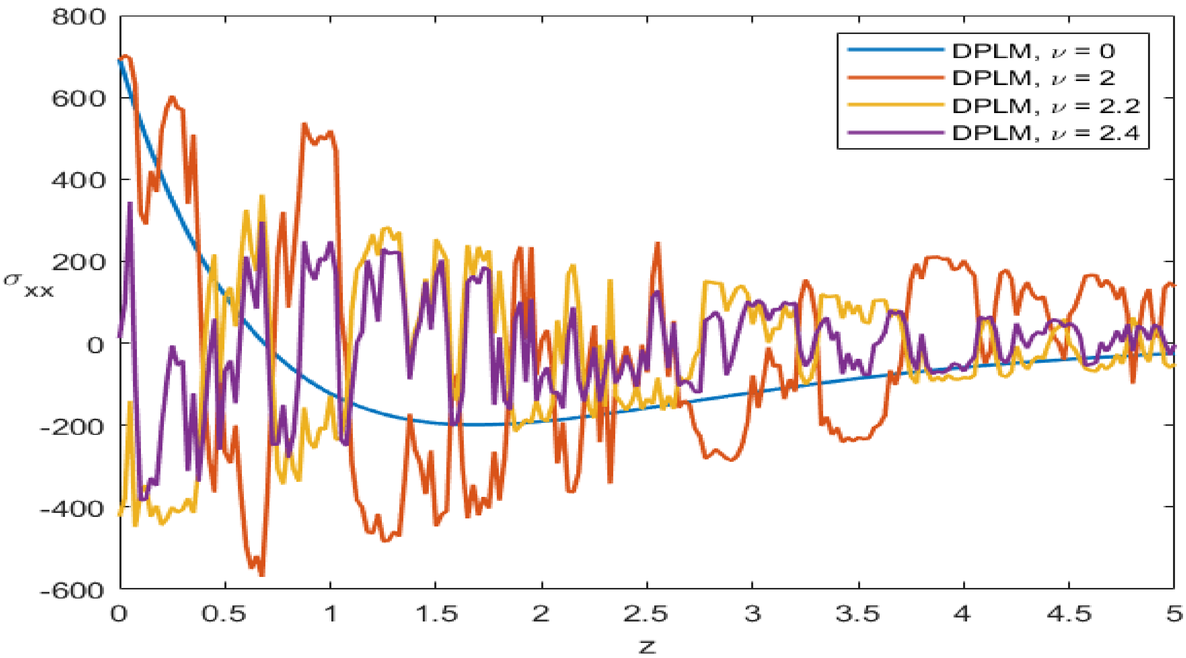

Figure 11. The stress tensor (σ_{xx}.) distributions for the DPLM

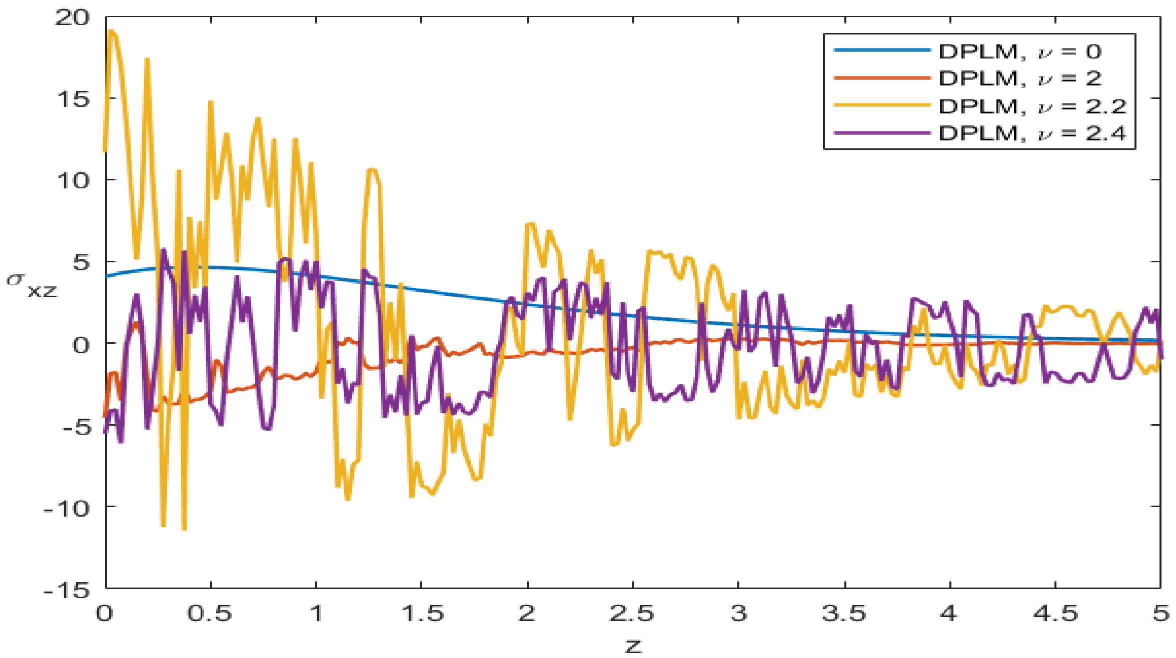

Figure 12. The stress tensor (σ_{xz}.) distributions for the DPLM

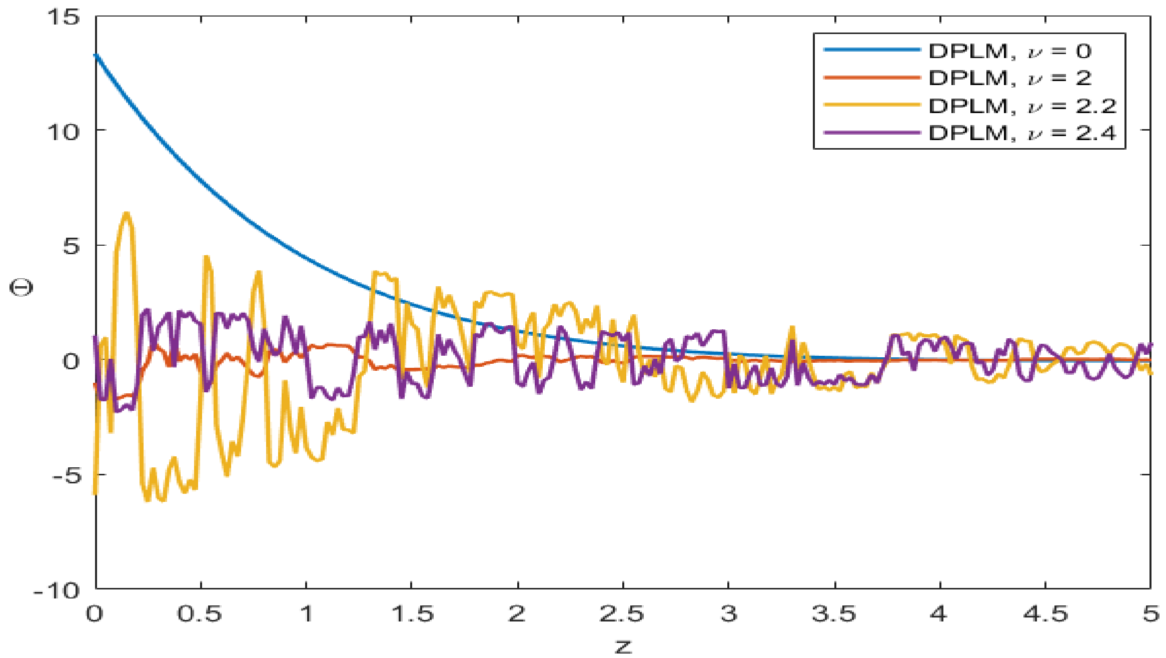

Figure 13. The temperature distributions for the DPLM

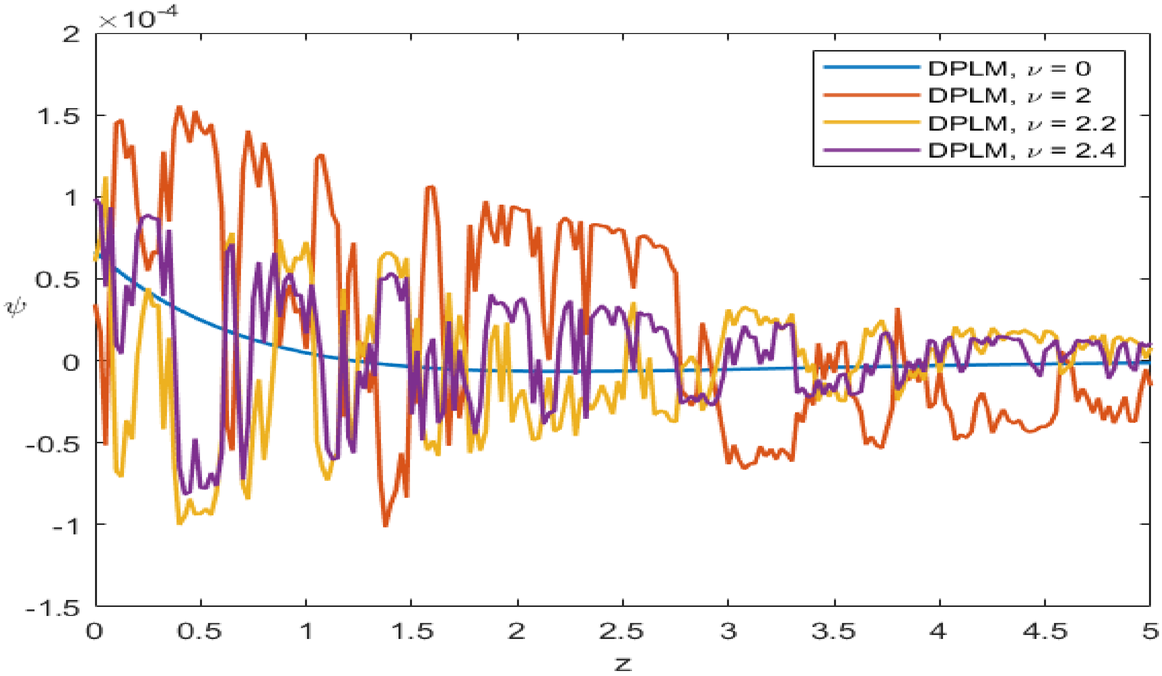

Figure 14. The micro-elongated distributions for the DPLM

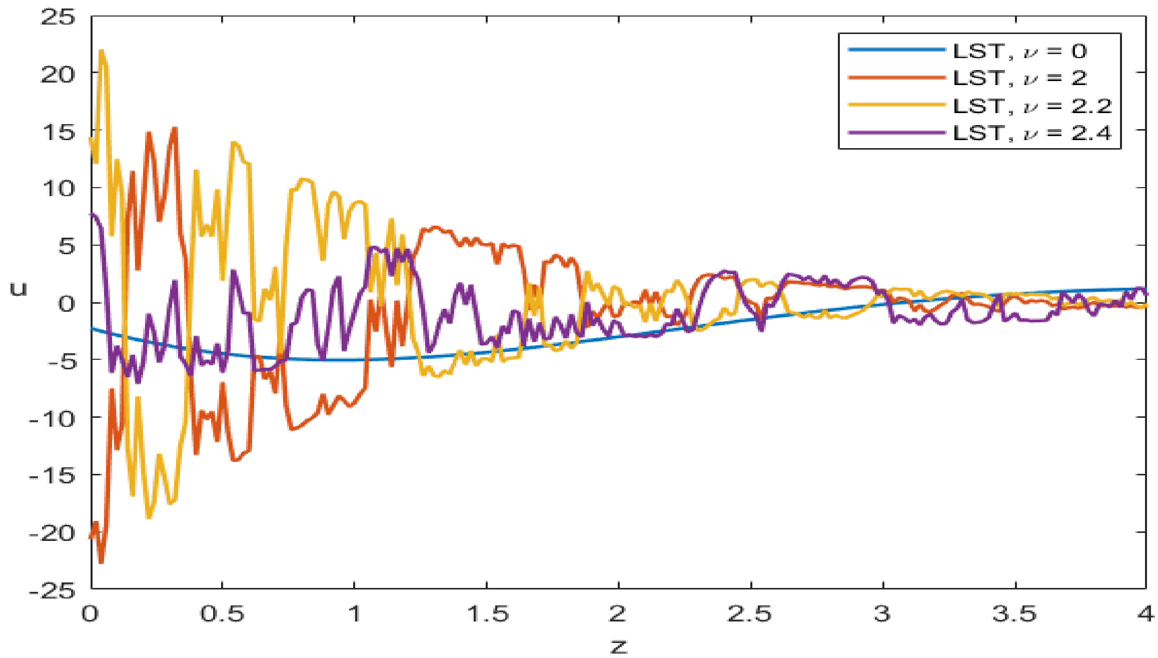

Figure 15. The horizontal displacement distributions for the LST

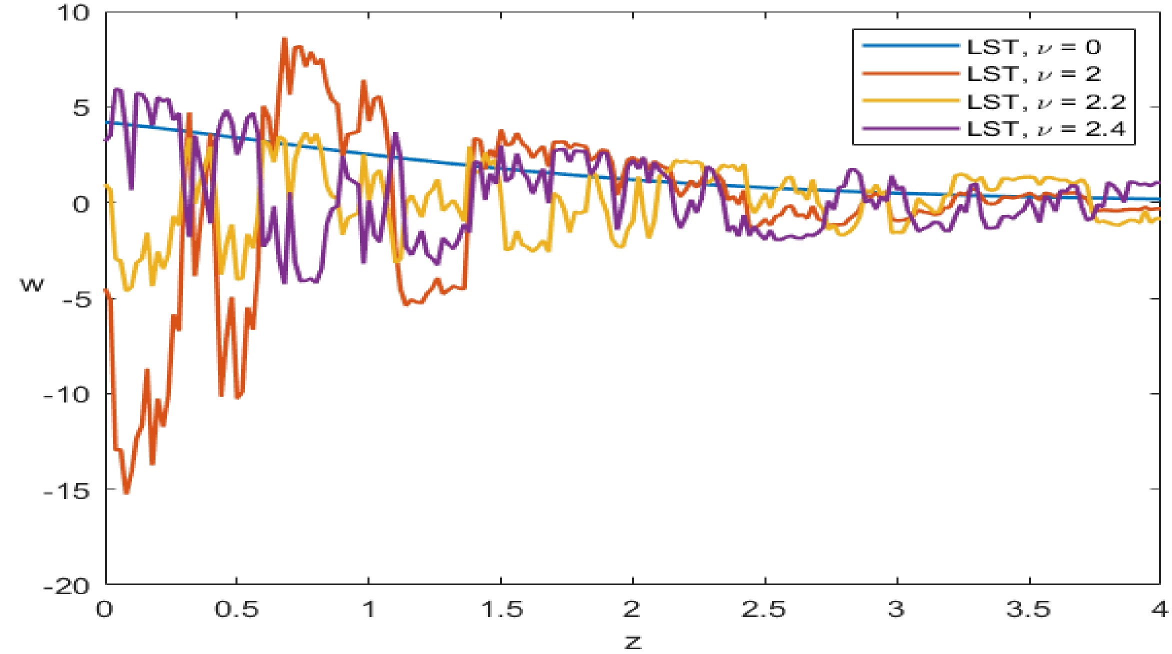

Figure 16. The vertical displacement distributions for the LST

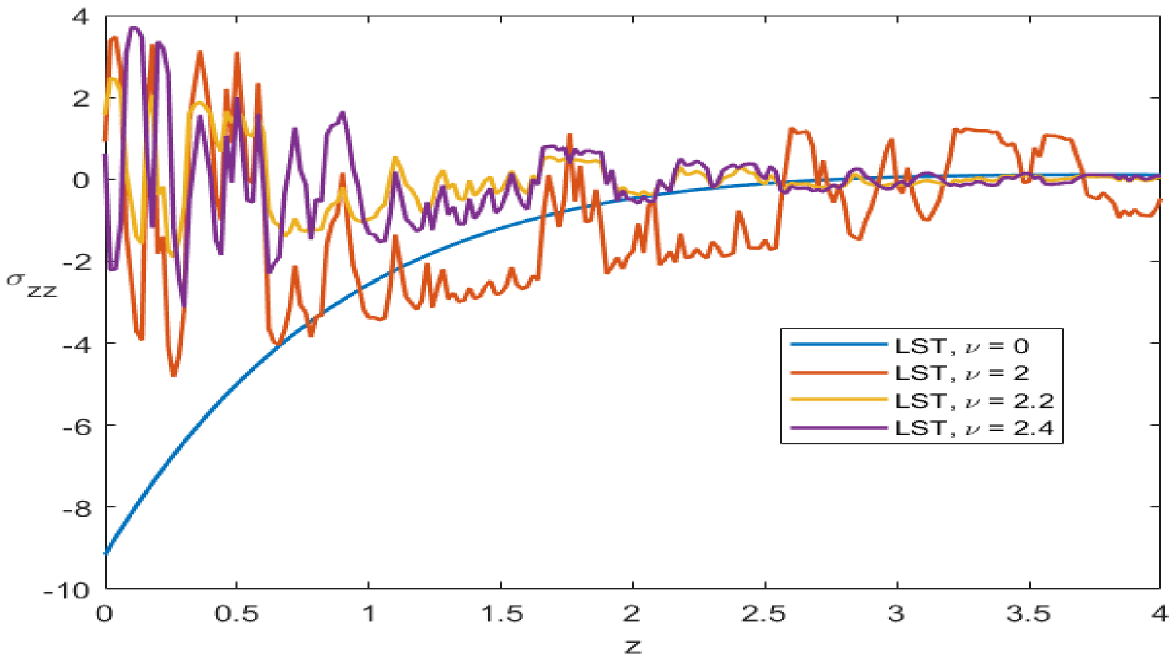

Figure 17. The stress tensor (σ_{zz}.) distributions for the LST

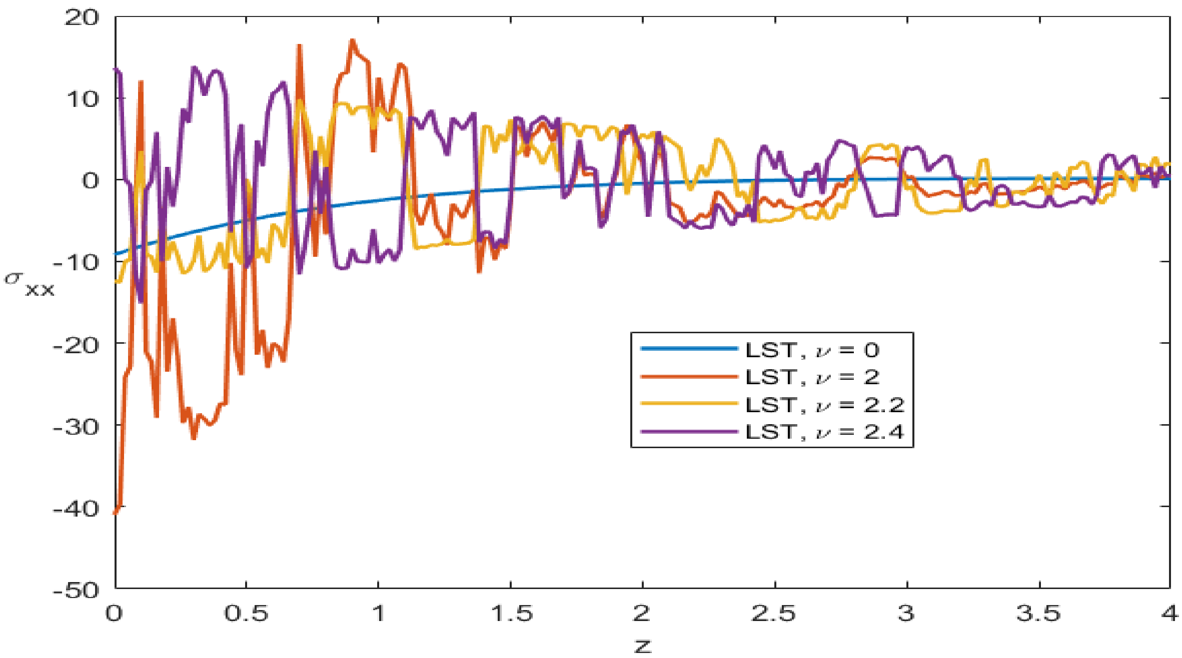

Figure 18. The stress tensor (σ_{xx}.) distributions for the LST

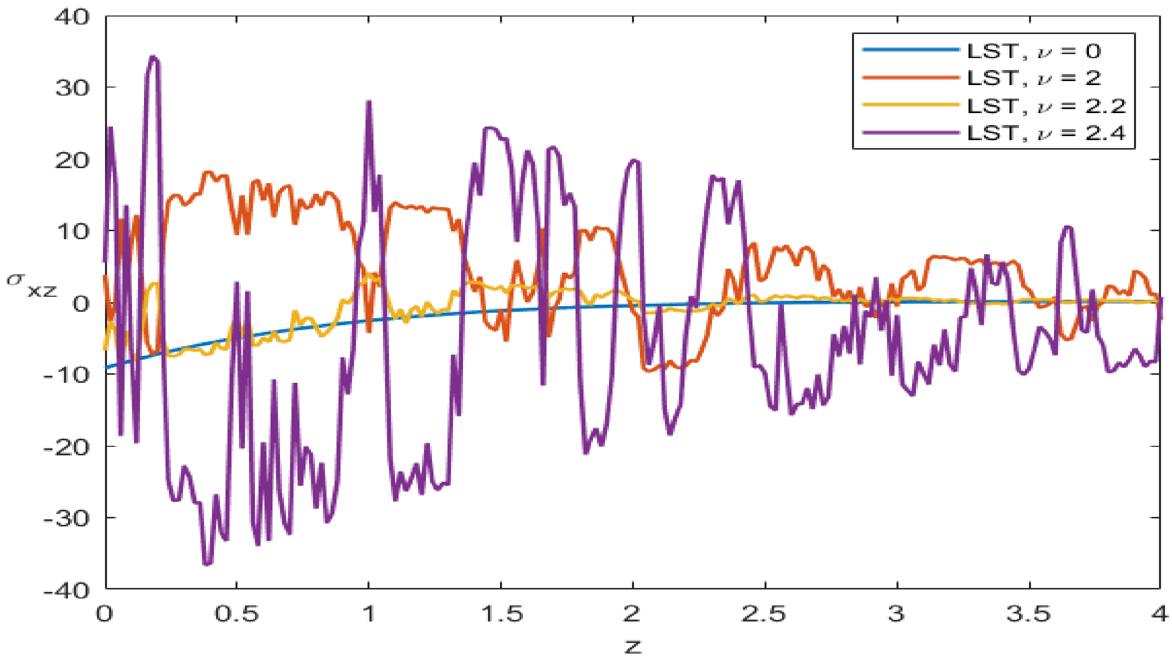

Figure 19. The stress tensor (σ_{xz}.) distributions for the LST

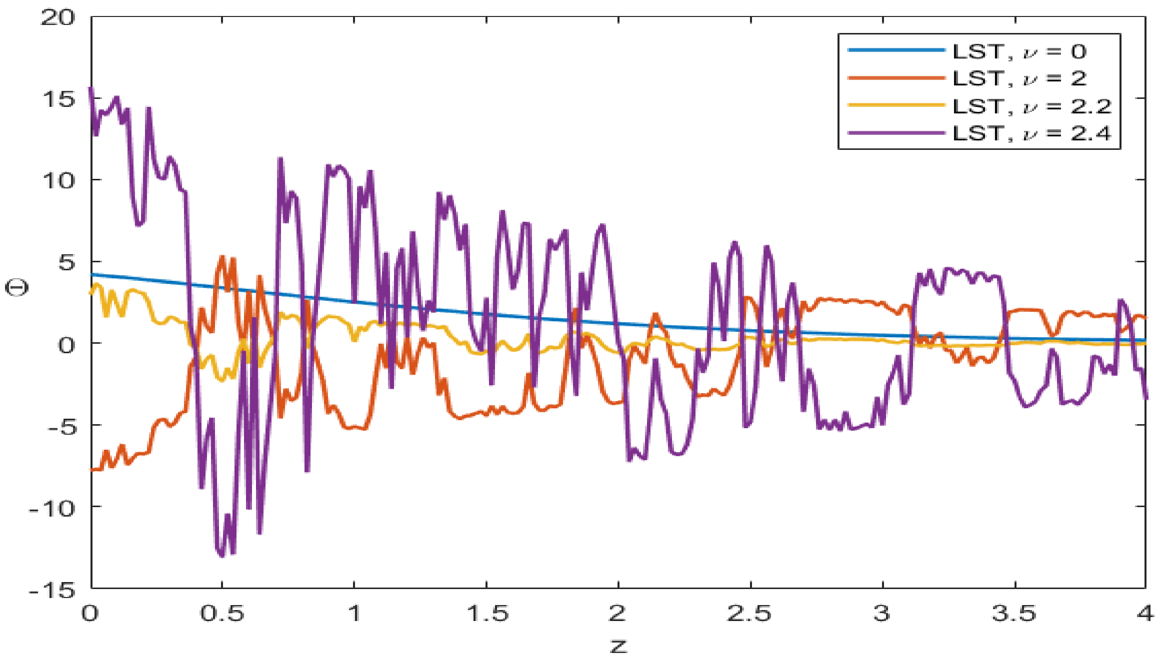

Figure 20. The temperature distributions for the LST

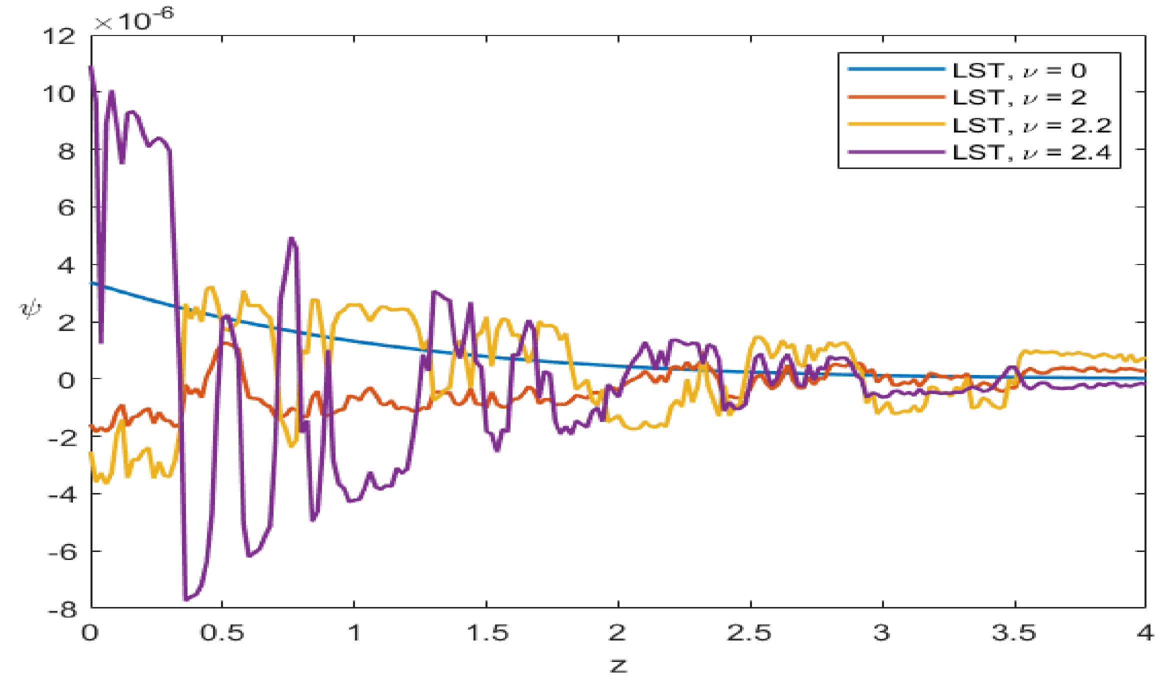

Figure 21. The micro-elongated distributions for the LST

6. Conclusion

This work provides a comprehensive analysis of the combined effects of stochastic thermal fluctuations on thermo-mechanical wave propagation in a micro-elongated thermoelastic half-space, examined within the frameworks of the LST, the DPLM, and the RDPLM. Starting from the fundamental governing equations of mechanical motion, heat conduction, and micro-elongation, the coupled system is reformulated and systematically reduced, through an appropriate transform technique, to a set of stochastic ordinary differential equations. This methodology enables the derivation of explicit analytical solutions for the temperature distribution, displacement fields, micro-elongation, and the corresponding stress components. Numerical simulations yield several significant physical insights. The incorporation of stochastic thermal excitation via a Wiener process leads to marked deviations from deterministic predictions, with random fluctuations becoming particularly pronounced in quantities that are strongly coupled to temperature, such as micro-elongation and thermally induced stresses. Comparative analysis among the three models reveals that the RDPLM demonstrates the highest sensitivity to stochastic disturbances, manifested by enhanced oscillatory behavior and pronounced wave-like thermal responses, attributable to its improved representation of finite-speed heat propagation and multiple phase-lag effects. The DPLM exhibits an intermediate level of sensitivity, while the LST displays the weakest response to stochastic perturbations, consistent with its more diffusive characterization of heat transport. Overall, these results underscore the importance of higher-order phase-lag models for accurately describing thermoelastic responses under random thermal loading, especially in microstructured materials where micro-elongation effects play a dominant role.

List of Nomenclatures

Quantity	Definition
$\mathbf{u}$	Displacement vector,
$\alpha_{t_1}, \alpha_{t_2}$	Coefficient of linear thermal expansion, where $\beta_0 = (3\lambda + 3\mu)\,\alpha_{t_1}, \beta_1 = (3\lambda + 3\mu)\,\alpha_{t_2}$,
λ and μ	Constants of Lame,
j^*	Microinertia,
T_0	Reference temperature,
$\lambda_0, \lambda_1, a_0$	Constants of micro-elongational,
ψ	Micro-elongational scalar,
Θ	Temperature,
c_e	Specific heat,
ρ	Density,
t	Time,
k	Thermal conductivity,
τ_θ	Phase-lag of the temperature gradient,
σ_{ij}	Component of stress tensor,
τ_q	Phase-lag of the heat flux.

Conflict of Interest

The authors declare there is no existing conflict of interest.

References

1.Abouelregal, A. E. (2021). Modified fractional thermoelasticity model with multi-relaxation times of higher order: application to spherical cavity exposed to a harmonic varying heat. *Waves in Random and Complex Media*, 31(5):812–832.

2.Ailawalia, P., Sachdeva, S. K., and Pathania, D. S. (2015). Plane strain deformation in a thermoelastic microelongated solid with internal heat source. *International Journal of Applied Mechanics and Engineering*, 20(4):717–731.

3.Allam, A. A., Ramadan, K. T., and Omar, M. (2016). A stochastic thermoelastic diffusion interaction in an infinitely long annular cylinder. *Acta Mechanica*, 227(5):1429–1443.

4.Alshehri, A. M., Lotfy, K., and Ibrahim, E. (2024). A novel model of microelongation thermomechanical photoacoustic waves in excited semiconductor materials. *Results in Physics*, 63:107881.

5.Ashraf, R., Amanat, F., Ashraf, F., Owyed, S., Matoog, R., Mahmoud, M., and Akgül, A. (2024). Soliton solutions for the (4+ 1)-dimensional fokas equation using integration techniques. *Alexandria Engineering Journal*, 107:61–72.

6.Bhattacharya, D. and Kanoria, M. (2024). Refined four-phase lag model for elasto-thermodiffusive interaction with harmonically varying heat sources. *Mechanics of Time-Dependent Materials*, 28(3):1853–1872.

7.Chiba, R. and Sugano, Y. (2007). Stochastic thermoelastic problem of a functionally graded plate under random temperature load. *Archive of Applied Mechanics*, 77(4):215–227.

8.Chiba, R. and Sugano, Y. (2008). Stochastic analysis of a thermoelastic problem in functionally graded plates with uncertain material properties. *Archive of Applied Mechanics*, 78(10):749–764.

9.El-Sapa, S., Alhejaili, W., Lotfy, K., and El-Bary, A. A. (2023). Response of excited microelongated nonlocal semiconductor layer thermomechanical waves to photothermal transport processes. *Acta Mechanica*, 234(6):2373–2388.

10.Hafed, Z. S., Abo-Dahab, S., Kilany, A., and Ahmed, S. E. (2025). Electromagnetic field on a photothermal semiconducting voids medium under lord–shulman and refined multi-phase lag models in thermoelasticity. *International Journal of Modern Physics B*, 39(01):2550007.

11.Hilal, M. I. (2022). Thermomechanical interactions of rotating thermoelastic magneto-microelongated medium heated by laser and initially stressed via non-local elasticity and gn iii. *Acta Mechanica*, 233(12):5183–5197.

12.Hosseini, S. M. and Shahabian, F. (2011). Stochastic assessment of thermo-elastic wave propagation in functionally graded materials (fgms) with gaussian uncertainty in constitutive mechanical properties. *Journal of Thermal Stresses*, 34(10):1071–1099.

13.Jeyaraman, P., Mahesh, S., Selvamani, R., Dimitri, R., Tornabene, F., et al. (2022). Multi thermal waves in a thermo diffusive piezo electric functionally graded rod via refined multi-dual phase-lag model. *Curved Layer. Struct*, 9(1):105–115.

14.Kadian, P., Kumar, S., Hooda, N., and Sangwan, M. (2024a). Reflection of plane waves in a non-local viscothermoelastic half-space under variable thermal conductivity and microelongation effects. *Journal of Thermal Stresses*, 47(11):1479–1499.

15.Kadian, P., Kumar, S., and Sangwan, M. (2024b). Effect of inclined mechanical load on a rotating microelongated two temperature thermoelastic half space with temperature dependent properties. *Journal of Vibration Engineering & Technologies*, 12(3):4053–4074.

16.Khamis, A., El-Bary, A., Lotfy, K., and Bakali, A. (2020). Photothermal excitation processes with refined multi dual phase-lags theory for semiconductor elastic medium. *Alexandria Engineering Journal*, 59(1):1–9.

17.Kutbi, M. A. and Zenkour, A. M. (2022). Refined dual-phase-lag green–naghdi models for thermoelastic diffusion in an infinite medium. *Waves in Random and Complex Media*, 32(2):947–967.

18.Lotfy, K. (2026). Thermo-mechanical waves of excited microelongated semiconductor layer during photothermal transport processes. *Waves in Random and Complex Media*, 36(1):690–706.

19.Lotfy, K., Ahmed, A., El-Bary, A., El-Shekhipy, A., and Tantawi, R. S. (2022). A novel stochastic photo-thermoelasticity model according to a diffusion interaction processes of excited semiconductor medium. *The European Physical Journal Plus*, 137(8):972.

20.Lotfy, K., Ahmed, A., El-Bary, A. A., Tantawi, R. S., Elidy, E. S., Saeed, A. M., and Mahdy, A. (2024). A stochastic photoacoustic study influenced by white noise on thermoelastic waves in semiconductor medium. *Semiconductors*, 58(12):948–959.

21.Mohammed, W. W., Cesarano, C., Alqsair, N. I., and Sidaoui, R. (2024). The impact of brownian motion on the optical solutions of the stochastic ultra-short pulses mathematical model. *Alexandria Engineering Journal*, 101:186–192.

22.Rezk, E. G., Ismail, G. M., Ahmed, A., Lotfy, K., El-Bary, A. A., Can, E., and Elidy, E. (2025). A stochastic dual-phase-lag two-temperature photo-thermoelastic model for double-porosity semiconductors with initial stress. *Scientific Reports*.

23.Sherief, H. H., El-Maghraby, N. M., and Allam, A. A. (2013). Stochastic thermal shock problem in generalized thermoelasticity. *Applied Mathematical Modelling*, 37(3):762–775.

24.Sherief, H. H., El-Maghraby, N. M., and Allam, A. A. (2017). Stochastic thermal shock problem and study of wave propagation in the theory of generalized thermoelastic diffusion. *Mathematics and Mechanics of Solids*, 22(9):1767–1789.

25.Zenkour, A. M. (2020). Thermo-diffusion of solid cylinders based upon refined dual-phase-lag models. *Multidiscipline Modeling in Materials and Structures*, 16(6):1417–1434.

26.Zenkour, A. M., Saeed, T., and Aati, A. M. (2023). Refined dual-phase-lag theory for the 1d behavior of skin tissue under ramp-type heating. *Materials*, 16(6):2421.